Cytoplasmic Viscosity Near the Cell Plasma Membrane: Translational Diffusion of a Small Fluorescent Solute Measured by Total Internal Reflection-Fluorescence Photobleaching Recovery

R. Swaminathan, S. Bicknese, N. Periasamy, and A. S. Verkman

Departments of Medicine and Physiology, Cardiovascular Research Institute, University of California, San Francisco, California 94143-0521 USA

ABSTRACT   Total internal reflection-fluorescence recovery after photobleaching (TIR-FRAP) was applied to measure solute translational diffusion in the aqueous phase of membrane-adjacent cytoplasm. TIR fluorescence excitation in aqueous solutions and fluorescently labeled cells was produced by laser illumination at a subcritical angle utilizing a quartz prism; microsecond-resolution FRAP was accomplished by acousto-optic modulators and electronic photomultiplier gating. A mathematical model was developed to determine solute diffusion coefficient from the time course of photobleaching recovery, bleach time, bleach intensity, and evanescent field penetration depth; the model included irreversible and reversible photobleaching processes, with triplet state diffusion. The validity and accuracy of TIR-FRAP measurements were first examined in aqueous fluorophore solutions. Diffusion coefficients for fluorescein isothiocyanate-dextrans (10–2000 kDa) determined by TIR-FRAP (recovery $t_{1/2}$ 0.5–2.2 ms) agreed with values measured by conventional spot photobleaching. Model predictions for the dependence of recovery curve shape on solution viscosity, bleach time, and bleach depth were validated experimentally using aqueous fluorescein solutions. To study solute diffusion in cytosol, MDCK epithelial cells were fluorescently labeled with the small solute 2',7'-bis-2-carboxyethyl-5-carboxyfluorescein-acetoxymethyl-ester (BCECF). A reversible photobleaching process ($t_{1/2} \approx 0.5$ ms) was identified that involved triplet-state relaxation and could be eliminated by triplet-state quenching with 100% oxygen. TIR-FRAP $t_{1/2}$ values for irreversible BCECF bleaching, representing BCECF translational diffusion in the evanescent field, were in the range 2.2–4.8 ms (0.2–1 ms bleach times), yielding a BCECF diffusion coefficient 6–10-fold less than that in water. These results establish the theory and the first experimental application of TIR-FRAP to measure aqueous-phase solute diffusion, and indicate slowed translational diffusion of a small solute in membrane-adjacent cytosol.

INTRODUCTION

The cytoplasm is a crowded aqueous compartment containing small solutes, macromolecules, and organized skeletal networks (Fulton, 1982; Clegg, 1984; Porter, 1984; Verkman, 1991; Luby-Phelps, 1994). The diffusional mobility of small solutes and macromolecules in cytoplasm has considerable importance in cell metabolism and signal transduction. For example, the translational diffusion of small solutes determines the rate at which ligands reach target enzymes, metabolites reach mitochondria, and nucleic acids reach the nucleus. The translation of small solutes may be of special importance in cytosol just beneath the plasma membrane to permit rapid signal transduction by G-protein-coupled mechanisms (Ausiello et al., 1987; Thomas et al., 1991). The diffusion of larger macromolecules is important for protein/protein and protein/nucleic acid interactions, as well as for the assembly of skeletal proteins into functional

networks required for organelle targeting and cell locomotion.

The central problem is to quantify the rates of translational and rotational diffusion of solutes in the cytosolic compartment. Because of spatial heterogeneity in the composition and organization of the cytosol, separate measurements are probably required for "bulk" cytosol, "peripheral" cytosol, and "membrane-adjacent" cytosol. The rheology of cytosol has been the subject of a series of biophysical investigations based on the analysis of viscosity-sensitive probes by electron spin resonance (Lepock et al., 1983; Mastro and Keith, 1984) and fluorescence spectroscopy (Luby-Phelps et al., 1986; Dix and Verkman, 1990; Fushimi et al., 1990). Two independent approaches have established recently that the "fluid-phase" cytoplasmic viscosity, defined as the viscosity sensed by a small molecule in the absence of collisions with or binding to cytosolic macromolecules (Verkman et al., 1991; Kao et al., 1993), is not much different from the viscosity of water. Fushimi and Verkman (1991) found that the picosecond rotational correlation times of aqueous-phase fluorescent probes in cytoplasm were only ~30% greater than that in water. Luby-Phelps et al. (1993) reached a similar conclusion using a "viscosity-sensitive" fluorophore whose quantum yield was sensitive to fluid-phase viscosity.

Kao et al. (1993) examined the translational mobility of a small fluorescent probe, 2',7'-bis-2-carboxyethyl-5-car-

boxyfluorescein-acetoxymethyl-ester (BCECF), in the cytoplasm of Swiss 3T3 fibroblasts, utilizing fluorescence recovery after photobleaching (FRAP). The translational diffusion of BCECF was ~4 times slower in bulk and peripheral cytosol than in water. Three independently acting factors were identified that accounted quantitatively for the slowed solute translation in cytosol compared to that in water: 1) slowed diffusion in fluid-phase cytosol, 2) probe binding to intracellular components, and 3) probe collisions with intracellular components. The latter factor, probe collisions, was determined to be the principal diffusive barrier that slowed small solute translation. Luby-Phelps et al. (1986) utilized FRAP to measure the translational diffusion of a series of microinjected, fluorescently labeled dextrans and ficolls. As the dextran or ficoll size was increased, diffusion in cytosol was decreased relative to that in water, suggesting a cytosolic "sieving" mechanism that was proposed to involve the skeletal mesh. Further studies in artificial solutions containing macromolecules and assembled F-actin networks have begun to resolve the factors that contribute to the apparent cytosolic sieving of macromolecules (Hou et al., 1990).

It has been proposed that the physical state of water in cytoplasm just beneath the plasma membrane is different from that in bulk or peripheral cytoplasm. Membrane-adjacent cytoplasm is a specialized region of cytosol bounded by a lipid membrane packed with integral proteins, as well as bound proteins that provide skeletal anchorage sites; this unique milieu has been proposed to cause partial or extensive organization of macromolecules, small solutes, and even water (Parsegian and Rau, 1984). Bicknese et al. (1993) utilized evanescent field frequency-domain microfluorimetry to quantify the picosecond rotational correlation time of small fluorescent probes in membrane-adjacent cytosol. Fluid-phase viscosity was probed within ~50 nm of the cell membrane by excitation of cytoplasmic BCECF fluorescence by total internal reflection (TIR). Probe rotation in membrane-adjacent cytosol did not differ significantly from that in bulk cytosol, in agreement with the conclusion that macromolecules (greater than ~5 kDa) have little influence on fluid-phase viscosity, as sensed by the microscopic motions of small molecules (Fushimi and Verkman, 1991; Periasamy et al., 1992). However, no information is available on the more important parameter, translational diffusion of solutes in membrane-adjacent cytoplasm.

The purpose of this study was to measure the translational diffusion of a small fluorescent probe in cytoplasm just beneath the plasma membrane. TIR was used to excite fluorescence selectively in membrane-adjacent cytoplasm, and FRAP was used to determine the kinetics of rapid fluorophore translation near the membrane. Although TIR-FRAP has been used to measure the kinetics of ligand binding to cell surfaces based on the generation of a fluorescence signal upon ligand binding (Axelrod et al., 1986; Hsieh and Thompson, 1994, 1995; Stout and Axelrod, 1994), it has not been used previously to study solute

diffusion in a three-dimensional aqueous phase. Because of the small penetration depth of the evanescent field produced by the TIR excitation, very fast recovery times were predicted. A microsecond FRAP apparatus consisting of acousto-optic modulators and a photomultiplier gating circuit was used to acquire TIR-FRAP recovery curves. A mathematical model of fluorescence recovery was developed that incorporated details of evanescent wave penetration, probe diffusion during and after the photobleaching pulse, and reversible photobleaching. The measurement of aqueous-phase solute diffusion by TIR-FRAP was validated in cell-free aqueous solutions and then applied in living cells to determine the BCECF translational diffusion coefficient. In performing the cell studies, an oxygen-dependent reversible photobleaching process that involved triplet-state relaxation was identified and characterized. Fortunately, it was found that the reversible photobleaching process could be effectively eliminated by carrying out cell measurements in a 100% oxygen atmosphere, permitting interpretation of the recovery signal in terms of BCECF diffusion. The results here provide the first measurement of solute translation in membrane-adjacent cytosol and establish the theory and technical details to examine the motion of larger solutes near biological interfaces.

MATERIALS AND METHODS

Cell culture

MDCK cells (passages 52–58, UCSF Cell Culture Facility) were grown on 18-mm-diameter round fused silica coverslips in DME-H21 medium supplemented with 5% fetal calf serum, penicillin (100 units/ml), and streptomycin (100 μg/ml). Fused silica was used to eliminate phosphorescence, which was found in all glass and sapphire coverslips tested. Cells were grown at 37°C in 95% air, 5% CO_2 and used 1–2 days after plating, at which time they were nearly confluent. Cells were loaded with BCECF-AM (Molecular Probes) by a 10-min incubation in culture medium.

Fluorescence microscopy

The output of an argon ion laser (488 nm, Innova 70-4; Coherent Inc.) was modulated by serial acousto-optic modulators (see below) and directed onto the stage of an inverted epifluorescence microscope (Diaphot, Nikon) (Fig. 1). The beam was focused by a 25× dry objective lens (working distance 1.6 cm, N.A. 0.35; Leitz) mounted on a four-axis micromanipulator, and directed to a fused silica right triangular prism (Melles-Griot). Light from the upper half of the objective was blocked to restrict the angular spread of the incident beam. The prism was in optical contact with the (cell-free) surface of the coverslip using spectroscopic grade glycerol. The beam incident angle was determined from the geometry of the optical configuration. Refractive indices of the prism and coverslip (n_{488nm} = 1.458) were used to calculate the incident angle at the dielectric:water interface. The focused laser beam produced an elliptical spot (~4 μm wide and ~70 μm long) in the sample plane. The sample and prism were positioned on the x,y translation stage of the microscope.

For measurements in aqueous solutions, 100-μl solution volumes were "sandwiched" between two coverslips using spacers. For cell measurements, the upper coverslip contained the cultured cells (facing downward). The sample was enclosed in a lucite chamber in which the atmosphere could be controlled (air or 100% nitrogen or 100% oxygen). In some experiments, the TIR prism was removed for direct ("trans") sample

FIGURE 1 Schematic of TIR-FRAP instrumentation. The beam from an Ar laser was modulated by serial acoustooptic modulators and directed onto the sample through a 25× objective lens and right triangular fused silica prism. The signal was filtered and detected by a gated photomultiplier. See text for details. (*Right*) Expanded view of prism showing beam incident angle ϕ and evanescent field depth d.
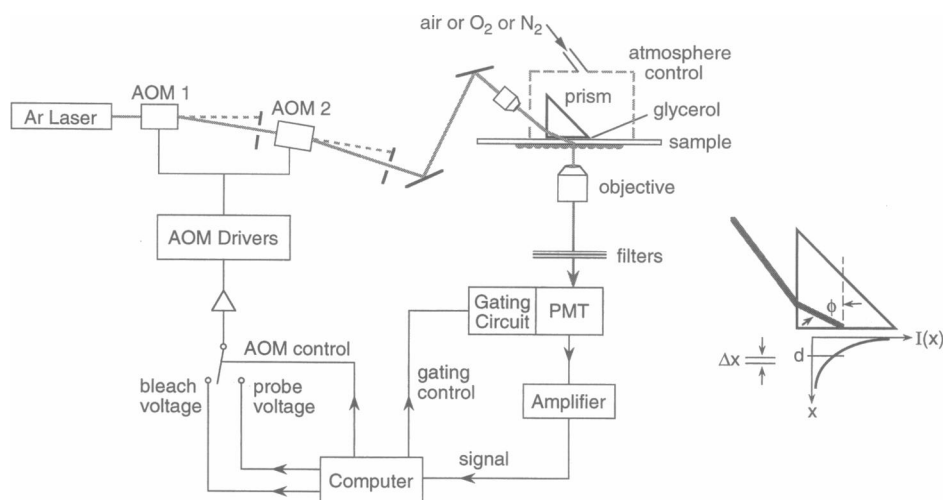
excitation, or the incident beam was directed along the optical axis of the microscope for conventional epiillumination (Verkman et al., 1991). Sample fluorescence was collected by an objective lens (20× dry, 0.75 N.A.; Nikon), passed through interference (520 ± 15 nm) and barrier (Schott glass OG 515) filters in series, and detected by a photomultiplier, the gain of which was software controlled (see below). The interference filter in the emission path was important for eliminating the detection of autophosphorescence of instrument components. No dichroic mirror was used for TIR and transillumination, and a 510 nm dichroic was used for epiillumination. In some experiments, TIR fluorescence images were acquired by a cooled CCD camera (imaging system described in Zen et al., 1992) utilizing a 100× water immersion objective (1.2 N.A.; Leitz) and an upright TIR microscope.

Fluorescence recovery after photobleaching

The laser beam was modulated by two acoustooptic modulators in series using 2-mm-diameter pinholes to isolate first-order beams (Kao and Verkman, 1996). Beam intensity was software modulated by intensity ratios of up to >10⁶:1, with rise and fall times of ~1.5 μs. For most TIR-FRAP experiments, the laser beam power was set to 0.1–0.3 W (488 nm), and the attenuation ratio (the ratio of the bleach beam intensity to the probe beam intensity) was set to 3,000–20,000. Fluorescence was detected by a photomultiplier (9828A; Thorn EMI) contained in a cooled housing (FACT50). Photomultiplier signals were amplified by a transimpedance amplifier (gain conversion 10^5 V/A, 1-μs rise time) and digitized at 1 MHz by using a 14-bit analog-to-digital converter. A gating circuit was used to transiently decrease photomultiplier gain for protection during the photobleaching pulse. The gating circuit was activated at 2 μs before the photobleaching pulse and deactivated at 3 μs after the pulse. The circuit switched the second dynode of the photomultiplier between its normal operating voltage and 108 V more negative than the first dynode, producing a ~1600-fold reduction in photomultiplier gain. The gating circuit generated a brief (~15 μs) anode current transient that was subtracted for measurement of very fast recovery curves.

Software was written in Microsoft QuickBasic 4.5 to record prebleach and postbleach signals, to modulate laser beam intensity, and to reduce photomultiplier gain during photobleaching. Signals were sampled before the bleach (generally 10^3 data points in 100 ms) and over three different time intervals after the bleach: high-resolution data (1 MHz sampling rate) over 10–100 ms, low-resolution data (generally 10^4 points) over 0.1–10 s, and "final signal" data (10^3 points) at late time after nearly complete recovery has occurred. High- and low-resolution data were binned into 200 points each for storage and analysis. The software permitted the rapid acquisition of multiple FRAP data sets for signal averaging. Generally,

data from 5–100 individual TIR-FRAP recovery curves were averaged; in cell studies, each recovery curve was obtained from a different spot.

MATHEMATICAL MODEL

In a FRAP experiment, a fraction of fluorophores in a small sample volume is bleached by a brief intense laser pulse. Fluorescence in the bleached volume decreases during the photobleaching pulse and then recovers as unbleached fluorophores diffuse into the bleached zone. For spot photobleaching in which fluorophore diffusion occurs in two dimensions, the time course of fluorescence recovery has been solved in analytical form (Axelrod et al., 1976), assuming a Gaussian or uniform circular profile without fluorophore diffusion during the bleach time, and subsequently with fluorophore diffusion (Bertch and Koppel, 1988). Recovery curves have been computed numerically where these assumptions are not valid (Lopez et al., 1988).

TIR-FRAP differs from spot photobleaching in two important aspects: the geometry of the bleach zone and the nature of interaction of light with the fluorophores. The intensity of the incident beam (during the bleach and probe times) decays exponentially in the sample with an exponential "distance constant" (d) that depends upon beam wavelength (λ) and incident angle (ϕ), and the refractive indices of the prism (n_p) and aqueous (n_{aq}) phases (Fig. 1, *right*; Axelrod et al., 1984; Hecht, 1987),

$$d = [\lambda/4\pi] (n_p^2 \sin^2\phi - n_{aq}^2)^{-1/2} . \tag{1}$$

Photobleaching therefore occurs only near the interface. Because d and hence the recovery time are very small, TIR-FRAP studies generally require a bleach time that is small compared to the recovery time. An additional factor for short bleach and recovery times is the presence of reversible photobleaching in which fluorescence recovery occurs in the absence of fluorophore diffusion. Reversible photobleaching is not fully understood, but may in part result from spontaneous and radical-induced recovery from

the triplet state (Velez and Axelrod, 1988; Scalettar et al., 1990; Corbett et al., 1994; Stout and Axelrod, 1995; Periasamy et al., 1996).

Because the two-dimensional beam spot size is much larger than the depth of the evanescent field, the TIR-FRAP diffusion-kinetic equation can be solved in one dimension,

$$dc/dt = D\, d^2c/dx^2 - kh(t)ce^{-x/d}, \qquad (2)$$

where $c(x, t)$ is the fluorophore concentration at distance x from the interface and time t, D (cm^2/s) is the fluorophore diffusion coefficient, k (s^{-1}) is a rate constant for irreversible photobleaching, and $h(t)$ is the step function: $h(t) = 1$ for $t < t_b$ (bleach time) and $h(t) = 0$ for $t > t_b$. The second term in Eq. 2 describes the intensity-dependent bleaching kinetics of the fluorophore during the bleach period, where $exp(-x/d)$ is the exponential decay of evanescent field intensity. It is assumed that beaching is a first-order process in which the bleaching efficiency depends linearly on light intensity. Equation 2 is subject to the initial condition $c(x, 0) = c_0$ and boundary condition $dc(0, t)/dx = 0$. The measured sample fluorescence [$F(t)$] is determined by integrating the product of $c(x, t)$ and the evanescent field intensity,

$$F(t) = F_0 \int c(x,t)\, e^{-x/d} dx, \qquad (3)$$

where the factor F_0 converts concentration to fluorescence.

Equation 2 assumes that the fluorophore exists in only two forms, fluorescent and irreversibly bleached. When reversible photobleaching occurs, as was found for rapid photobleaching studies in cells, the right-hand term in Eq. 2 contains two additional terms: $-k_t e^{-x/d}h(t)c(x, t) + k_T c_T(x, t)$. The first term describes the formation of triplet state fluorophore during the bleach time with rate constant k_t (s^{-1}). The second term represents triplet decay to the active (nonbleached) ground state, where k_T (s^{-1}) is the rate of triplet decay and $c_T(x, t)$ is the triplet concentration profile. It is noted that a second diffusion equation (similar to Eq. 2) is required to describe $c_T(x, t)$ diffusion.

Equation 2 was solved numerically by a discretization procedure similar to that developed for electrochemical diffusion/reaction problems (Feldberg, 1969). Volume elements were taken of thickness Δx parallel to the dielectric interface located at $x = 0$. At $t = 0$, $c(x, 0) = c_0$. During each time interval Δt, kinetic processes (irreversible and reversible photobleaching) occur in each volume element, and fluorophore diffusion occurs in accordance with Fick's law. For discretization, the bleach time (t_b, typically 100–5000 μs) was divided into N (generally 10^3) equal intervals. Δx was chosen to approximate the characteristic diffusion distance $(2D\Delta t)^{1/2}$. Δt was chosen to be sufficiently small such that $\Delta x < 0.1\, d$.

Fluorophore concentration $c(x, t)$ in each volume element was calculated for the kinetic and diffusive processes. The kinetic term for the ith volume element from the interface is

$$c(x_i, t_j + \Delta t) = c(x_i, t_j)\,[1 - h(t_j)\, g_B \Delta t e^{-x/d}], \qquad (4)$$

where g_B is the bleach rate determined to give a specified bleach efficiency. Fluorophore diffusion from x_i to each x-element during time interval t_j to $t_j + \Delta t$ is

$$c(x_{i+m}, t_{j+1}) = 0.5(\pi D\Delta t)^{-1/2}c(x_i, t_j)exp(-m^2\Delta x^2/4D t_j). \qquad (5)$$

The diffusion of the molecules near the interface is treated by application of reflection boundary conditions (Chandrasekar, 1943). For calculations, Eqs. 4 and 5 were applied at each t_j with a maximum x depth of $8d$. The computed x and t profiles were insensitive to a fivefold decrease in Δx and Δt, and agreed quantitatively with analytical solutions to the diffusion equation where the kinetic term was excluded.

The presence of a fluorophore-free aqueous layer of thickness h and refractive index $n_r = 1.333$ between the silica ($n_r = 1.458$) and cytoplasm ($n_r = 1.38$) was incorporated into the TIR-FRAP model by shifting the $x = 0$ plane to the water/cell interface (see Fig. 7 A, left) and including the appropriate equation for evanescent field intensity decay. As detailed in Gingell et al. (1987), theory predicts that the evanescent field intensity decays exponentially in the cytoplasm with distance constant d given by Eq. 1. The intensity at the water/cytoplasm interface (ignoring the $\sim$4-nm-thick membrane phase) is determined from the thickness of the aqueous layer, refractive indices, wavelength, and beam incident angle.

For experimental determination of solute diffusion coefficient D, measured $F(t)$ was fitted to simulated $F(t)$ (by least squares), in which D was varied with fixed experimental parameters (bleach time, evanescent field penetration depth, and bleach depth; see below). $F(t)$ at infinite time was taken as 1 for cell-free solution studies and as $F(100$ $t_{1/2})$ in cell experiments.

RESULTS

Predictions of the mathematical model

The major predictions of the mathematical model for TIR-FRAP are shown in Fig. 2. The four independent, experimentally relevant parameters (in the absence of reversible photobleaching) include fluorophore diffusion coefficient (D), evanescent field penetration depth (d), bleach time (t_b), and bleach efficiency (g_B). The bleach depth, defined as the decrease in fluorescence intensity at the end of the bleach pulse, is determined by the four independent parameters and can be specified by adjusting parameter g_B. The bleach depth was generally set to 20% for the simulations unless otherwise specified.

Fig. 2 A shows the time evolution of the fluorophore x concentration profile [$c(x, t)/c_0$] during a 250-μs bleach period for $D = 10^{-6}$ cm^2/s and $d = 100$ nm. Because of fluorophore diffusion during the bleach pulse, there is with increasing bleach time an increase in bleach depth at the TIR interface ($x = 0$) as well as in the x penetration of the bleach profile. Fig. 2 B shows the corresponding fluorophore x concentration profiles during the probe (recovery)
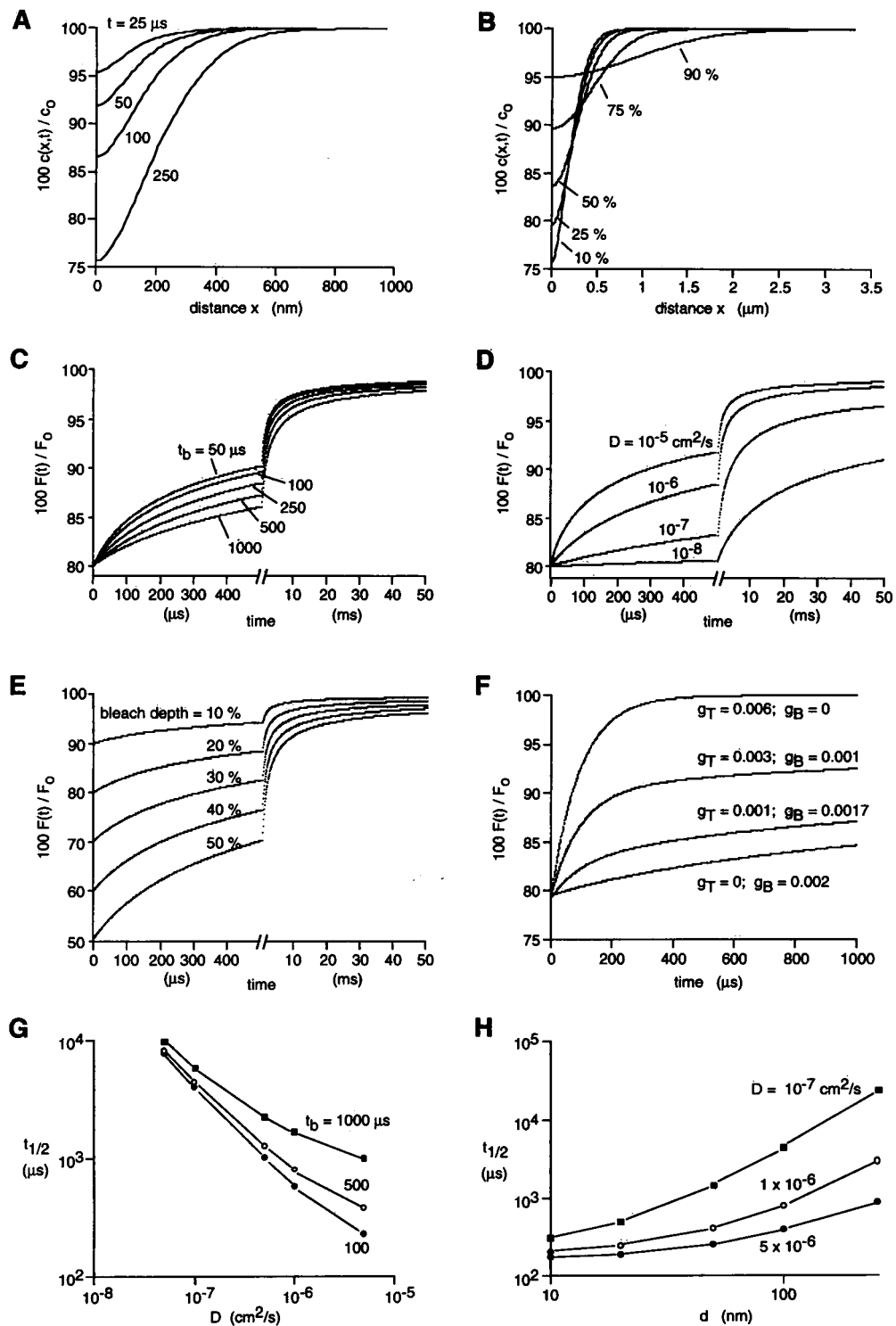
FIGURE 2   Predictions of the mathematical model for calculation of TIR-FRAP recovery curves. (A) Fluorophore x concentration profiles [$c(x, t)/c_o$] at indicated times during bleach for $D = 10^{-6}$ cm^2/s and $d = 100$ nm. At 250 μs, the fluorescence intensity [$F(t)$] was 80% of the initial intensity. (B) Concentration profiles at indicated times during fluorescence recovery after a 250-μs bleach. Curves correspond to times at which the fluorescence has recovered by 10%, 25%, 50%, 75%, and 90%. Parameters are the same as in A. (C) $F(t)$ as a function of bleach time (t_b) for $D = 10^{-6}$ cm^2/s, $d = 100$ nm, and g_B adjusted to give 20% bleach depth. (D) Recovery curves as a function of fluorophore diffusion coefficient (D) for $d = 100$ nm and $t_b = 100$ μs. Bleach efficiency (g_B) was adjusted to give 20% bleach depth. (E) $F(t)$ as a function of bleach depth (by varying g_B) for $t_b = 250$ μs, $D = 10^{-6}$ cm^2/s, and $d = 100$ nm. (F) $F(t)$ in the presence reversible photobleaching with $t_T = 100$ μs, $D = 10^{-7}$ cm^2/s, $t_b = 250$ μs, and $d = 100$ nm. Parameters g_T and g_B were adjusted to vary the fractional recovery due to reversible photobleaching and to maintain 20% bleach depth. (G) Log-log plot of $t_{1/2}$ versus D for simulated fluorescence recovery curves with indicated t_b for $d = 100$ nm and 20% bleach depth. (H) Dependence of $t_{1/2}$ on d for simulated recovery curves with indicated D for $t_b = 250$ μs and 20% bleach depth.

period, at times when the fluorescence intensity has recovered by 10, 25, 50, 75, and 90% (see legend). Fluorophore concentration near the interface, and thus $F(t)$, increases with time, whereas, interestingly, fluorophore concentration far from the interface decreases with time. The concentration profile returns to the prebleach profile [$c(x, t)/c_o = 1$] only at infinite time; however, in practice, convective transport would dominate diffusional transport at very long times.

Fig. 2 C shows the dependence of the fluorescence recovery curves [$F(t)$] on bleach time (t_b) for fixed d and D (see legend for parameter values). The fluorescence recovery is clearly nonexponential, having a rapid initial phase followed by remarkably slow recovery at later times. The early rise in $F(t)$ is slowed with increasing t_b because of fluorophore diffusion during the bleach time, as seen in Fig. 2 A. Fig. 2 D demonstrates the sensitivity of $F(t)$ to fluorophore diffusion coefficient (D) for fixed d and t_b. The recovery profiles differ remarkably, providing the theoretical basis for the experimental determination of D by TIR-FRAP. Fig. 2 E shows $F(t)$ for different bleach depths in the range 10–50%, with a bleach period of 250 μs and fixed D and d. Although the amplitudes of the recovery profiles differ, the recovery curve shape (e.g., recovery half-time) generally depends weakly on bleach depth.

The simulations in Fig. 2, A–E, were carried out for fluorophore photobleaching by an exclusively irreversible mechanism (Eqs. 1–3). Fig. 2 F shows the influence on recovery curve shape of an additional reversible photobleaching process (Eqs. 4 and 5) involving the formation and decay of triplet state fluorophore defined by two parameters: triplet-state formation efficiency (g_T) and triplet-state lifetime ($t_T = 1/k_T$). The diffusion coefficient of the triplet was assumed for the simulation to be identical to that of the ground state. The parameters for the simulation in Fig. 2 F were $t_T = 100$ μs, $D = 10^{-7}$ cm^2/s, $t_b = 250$ μs, and $d = 100$ nm, with bleach depth set to 20%. The fractional recovery due to reversible photobleaching was varied by adjusting parameters g_T and g_B. In the absence of irreversible bleaching ($g_B = 0$), the rapid fluorescence recovery was due entirely to triplet decay. For this simulation $t_{1/2}$ was 67 μs, in agreement with the theoretical value of 69 μs. As the fractional recovery due to irreversible photobleaching increases ($g_B > 0$), the fluorescence recovery assumes the mixed character of the two mechanisms. Recovery due to a purely irreversible bleaching mechanism involving fluorophore diffusion ($g_T = 0$) is relatively slow. This simulation underscores the need to evaluate whether reversible photobleaching processes are occurring for experimental determination of fluorophore diffusion by photobleaching recovery techniques (Periasamy et al., 1996).

Fig. 2 G shows the influence of D on recovery half-time ($t_{1/2}$), defined as the time at which $F(t)$ is equal to [1 + $F(0)$]/2. Simulations were carried out for various beach times (t_b) with a fixed d of 100 nm. As in the simulations above, the bleach depth was maintained at 20% by adjusting g_B, which is equivalent to experimentally setting laser beam

intensity to maintain a specified bleach depth. The plot demonstrates that $t_{1/2}$ is most sensitive to changes in D for small t_b. Experimentally, bleach times should thus be smaller than or similar to recovery times to measure D accurately and to restrict the effective penetration depth of bleach pulse. Fig. 2 H shows the dependence of $t_{1/2}$ on evanescent field depth (d). Whereas $t_{1/2}$ is relatively insensitive to changes in d for high D (5 × 10^{-6} cm^2/s), $t_{1/2}$ becomes very sensitive to d for small D. A plot of $t_{1/2}$ versus d is therefore potentially useful for accurate determination of D by TIR-FRAP; however, in practice, the range of attainable values for d is limited with variable-angle TIR, particularly when an objective lens is used to increase beam intensity.

TIR-FRAP measurements in aqueous solutions

Experiments were first carried out in cell-free aqueous solutions to validate the measurement of fluorophore diffusion by TIR-FRAP. Fig. 3 A shows TIR-FRAP recovery curves for a series of fluorescein isothiocyanate (FITC)-labeled dextrans in the molecular mass range 10–2000 kDa. Measurements were performed with a 100-μs bleach time and an incident laser beam angle of 77° at the quartz-aqueous interface, producing an evanescent field of penetration depth $d = 112$ nm. Beam intensity was adjusted to produce ~20% bleaching. Monophasic recovery curves were detected with increasing recovery half-times ($t_{1/2}$) for the dextrans of increasing molecular size. Fluorescence returned to near-initial levels, indicating that essentially all of the aqueous fluorophore was mobile; furthermore, the complete recovery indicates that the signal arose exclusively from emission of fluorophore excited by TIR, because any component of trans (non-TIR) excitation would result in incomplete recovery over a short time scale. Fig. 3 B shows recovery curves obtained for the same aqueous solutions by spot photobleaching (by epiillumination) using a 20× objective. The recovery time course for spot photobleaching was remarkably slower than that for TIR-FRAP because of the greater characteristic diffusion distance (~2000 nm for spot photobleaching versus <200 nm for TIR-FRAP). Diffusion coefficients (D) determined from analysis of the FRAP data as described in Materials and Methods showed very good agreement in calculated D values obtained by spot photobleaching and TIR-FRAP (Fig. 3 C). For comparison, D values for small solutes (e.g., glucose) are ~5 × 10^{-6} cm^2/s.

The validity of the TIR-FRAP method was next examined for a wider range of bleach parameters and solution compositions. Fig. 4 A shows recovery curves obtained from aqueous solutions of fluorescein made viscous with glycerol. The recovery was remarkably slowed with increasing solution viscosity. Calculated D values were 2.6 × 10^{-6} and 1.0 × 10^{-6} cm^2/s for solutions of relative viscosities of 1 (phosphate-buffered saline, PBS) and 2.9 (34% glycerol), in agreement with the Stokes-Einstein relation. Interestingly, at high glycerol (49%), an additional fast component
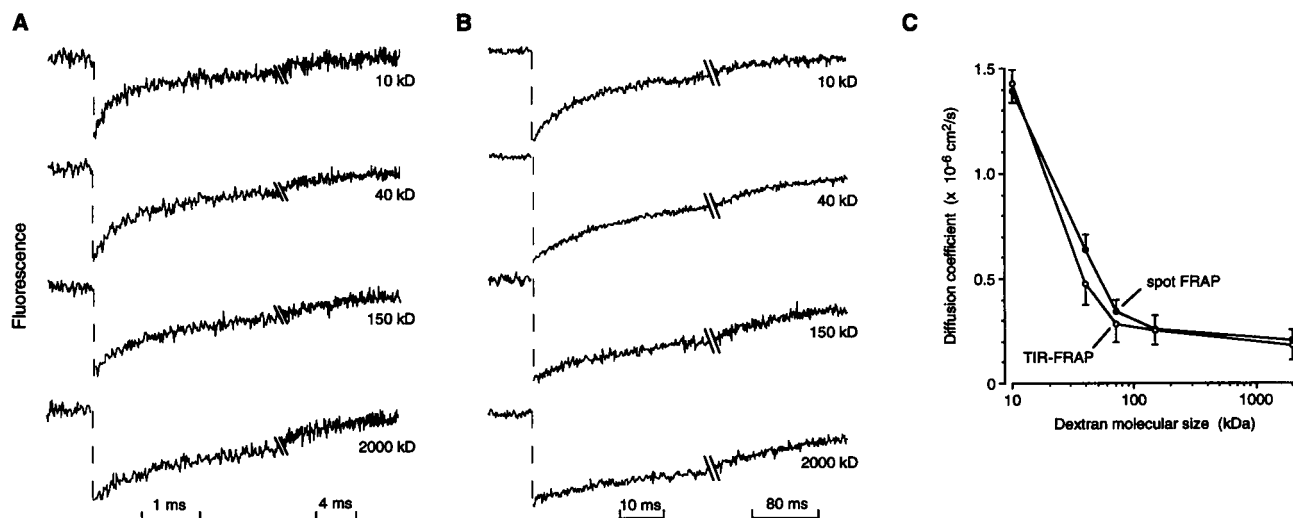
FIGURE 3   TIR-FRAP determination of diffusion coefficients of FITC-labeled dextrans. TIR-FRAP (A) and spot photobleaching (B) recovery curves for FITC-dextrans (2 mg/ml) of indicated molecular size in PBS. For TIR-FRAP, t_b = 100 μs, d = 80 nm, and laser beam intensity was adjusted to give ~20% bleach depth. For spot photobleaching, the spot was produced by a 20× objective (spot diameter ~4 μm) in an epiillumination configuration with a bleach time of 1 ms. (C) Comparison of computed solute diffusion coefficients D determined by TIR-FRAP and spot photobleaching.

of recovery appeared ($t_{1/2}$ ≈ 75 μs) that was too fast to be ascribed to solute diffusion. This process arose from reversible photobleaching of the fluorescein triplet state in viscous nondeoxygenated solutions (Periasamy et al., 1996); an identical fast component of recovery was observed in the same sample when the TIR laser spot was defocused, and in spot photobleaching (not shown), indicating its origin from a nondiffusive process. After subtraction of the (assumed single exponential) reversible photobleaching component, the TIR-FRAP measurement of fluorescein diffusion in the 49% glycerol solution (relative viscosity 6.4) gave a D value of 0.5 × 10^{-6} cm^2/s. In subsequent TIR-FRAP measure-

ments in cells below, the contribution of reversible photobleaching to the observed recovery was investigated by removing the quartz prism to effect trans (non-TIR)-illumination in which no significant diffusion-related recovery should occur (because many individual fluorescently labeled cells are illuminated).

Fig. 4, B and C, shows the dependence of TIR-FRAP recovery on bleach time and depth. The bleach time study was particularly important because it constitutes the most stringent test of the model. Recovery slowed and recovery curve shape changed with increasing bleach time (Fig. 4 B); however, fitted D values remained unchanged (in cm^2/s ×
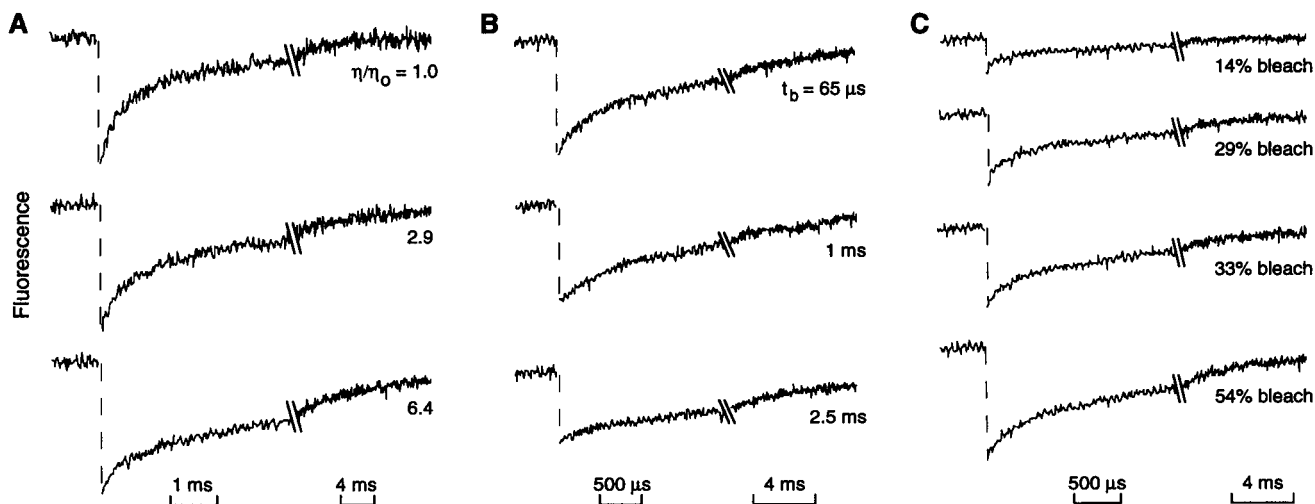

FIGURE 4   Dependence of TIR-FRAP recovery curve shape on solution viscosity, bleach time, and bleach depth. (A) Solutions contained 1 mM fluorescein in PBS with 0%, 34%, or 49% glycerol, giving relative viscosities (η/η_o) of 1, 2.9, and 6.4, respectively. TIR-FRAP parameters: t_b = 65 μs, incident beam angle 77°, and bleach depth ~20%. (B) Bleach time t_b was varied for fluorescein in PBS with parameters as above. (C) Bleach depth was varied at a constant t_b of 65 μs by change in laser illumination intensity.

10^{-6}): 2.8 (t_b 65 μs), 2.3 (1 ms), and 2.6 (2.5 ms). In contrast, there was little change in recovery curve shape (only amplitude) with increasing bleach depth as predicted by the model; D values (in cm^2/s $\times$ 10^{-6}) were 2.3 (14% bleach depth), 2.6 (29%), 3.0 (33%), and 2.6 (54%). Taken together, these results establish the validity of TIR-FRAP for the measurement of solute diffusion coefficient near a TIR interface.

Solute diffusion in fluorescently labeled cells

Initial TIR-FRAP measurements of BCECF-labeled MDCK cells revealed a large-amplitude recovery process with a recovery half-time of 1–2 ms. The fast recovery was surprising because it implied that BCECF diffusion in cytosol was similar to that in water, a result clearly inconsistent with previous spot photobleaching data (Kao et al., 1993). However, further studies by transillumination (where little or no recovery was expected) and by epiillumination (where slow recovery over tens of milliseconds was expected) revealed the same fast recovery process (see Fig. 5 A, top curve). The recovery process thus did not depend upon solute diffusion and had to be understood and/or eliminated to determine the diffusion coefficient of BCECF in membrane-adjacent cytosol.

Various types of reversible photobleaching have been described previously, including microsecond recovery in oxygenated solutions (Velez and Axelrod, 1988; Scalettar et al., 1990; Corbett et al., 1994) and slow (hundreds of milliseconds) recovery of an immobilized fluorophore (Stout and Axelrod, 1995). We recently characterized a reversible photobleaching process for fluorescein in air-saturated viscous aqueous solutions that involved triplet state formation and decay, and could be strongly accelerated by the addition of triplet-state quenchers, including oxygen, tryptophan, and manganese (Periasamy et al., 1996). Reversible photobleaching was also observed for fluorescein-macromolecule conjugates and depended upon the detailed environment of the fluorophore and the oxygen diffusion coefficient in the aqueous medium. We concluded that the fast recovery observed for BCECF in MDCK cells also involved triplet-state formation, and if so, it might be eliminated by triplet-state quenchers such as oxygen.

Fig. 5 shows photobleaching studies performed in BCECF-labeled cells bathed in solutions saturated with air, 100% nitrogen, or 100% oxygen. Measurements were carried out by transillumination (with the TIR prism removed) to minimize recovery due to solute translational diffusion. The reversible photobleaching process was observed using a short photobleaching time, relatively low bleach beam illumination intensity, and rapid data acquisition (Fig. 5 A). The recovery process was increased in amplitude and slowed in the nitrogen-saturated buffer, but was essentially eliminated in the oxygen-saturated solution. Further studies showed that fast process was not affected by beam focus, decreased in amplitude with increasing bleach time, and was eliminated by 0.5% hydrogen peroxide (data not shown). Taken together, these results implicate a reversible photobleaching process that involves triplet-state formation and oxygen-dependent triplet decay (see Discussion). Oxygen-saturated solutions were thus used in subsequent TIR-FRAP measurements to eliminate reversible photobleaching. The irreversible photobleaching process was observed using a longer photobleaching time and relatively high beam illumination intensity (Fig. 5 B). As predicted (Song et al., 1995), the efficiency of irreversible photobleaching was increased by oxygen.

To measure BCECF translation in bulk cytosol (to compare with data in membrane-adjacent cytosol) and to determine whether 100% oxygen affects BCECF diffusion, FRAP measurements were carried out by epiillumination (Fig. 6 A). Measurements in air-saturated solutions showed a recovery $t_{1/2}$ value of 33 $\pm$ 2 ms (n = 6) with ~60% recovery. Taken together with calibration measurements performed in aqueous solutions of known viscosity (as described in Kao et al., 1993), the BCECF diffusion coefficient in bulk cytosol was 3.8-fold less than that in aqueous solution. Fig. 6 A (bottom curve) demonstrates no significant effect of 100% oxygen on BCECF diffusion ($t_{1/2}$ = 32 $\pm$ 3 ms, n = 6).

Fig. 6 B shows TIR-FRAP measurements of BCECF diffusion in MDCK cells bathed in an oxygen-saturated solution. The three curves show similar recovery kinetics for different photobleaching times (t_b), each much shorter than the average recovery $t_{1/2}$ of ~4.5 ms. Corresponding experiments performed by transillumination showed no

FIGURE 5 Oxygen dependence of reversible and irreversible photobleaching of BCECF in MDCK cells. MDCK cytoplasm was loaded with BCECF as described in Materials and Methods. Cells were bathed in PBS equilibrated with air, 100% oxygen, or 100% nitrogen. Photobleaching was performed in the *trans* configuration. (A) Reversible photobleaching obtained with 250-μs bleach time and low laser beam intensity. (B) Irreversible photobleaching obtained with 1-ms bleach time and high laser beam intensity. Note the disappearance of the reversible photobleaching signal and increased efficiency for irreversible photobleaching in the presence of 100% oxygen.
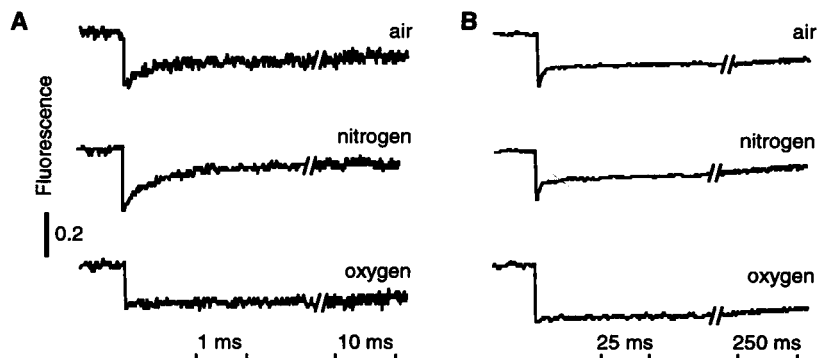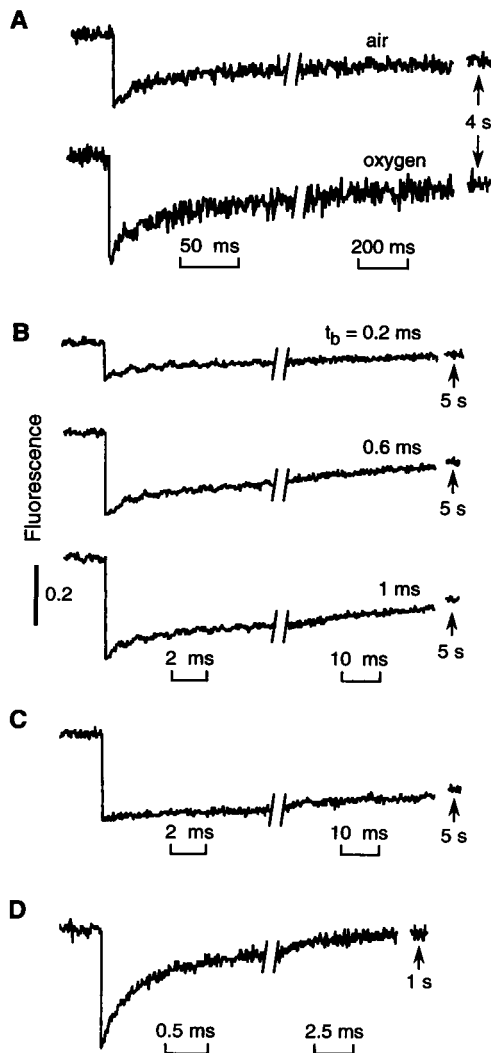
FIGURE 6 Translational diffusion of BCECF in MDCK cytosol measured by spot photobleaching and TIR-FRAP. (A) Spot photobleaching measurement by epiillumination using a 20× dry objective. Bleach time was 1 ms. Cells were bathed in PBS equilibrated with air (top curve) or 100% oxygen (bottom curve). In this and subsequent curves, the averaged fluorescence at the indicated late time (after which essentially all recovery has occurred) is shown. (B) TIR-FRAP measurements with indicated bleach times. (C) Measurement identical to that in B (1-ms bleach time) with prism removed (for *trans* illumination). (D) TIR-FRAP measurement of diffusion of fluorescein (1 mM) in PBS with 0.1-ms bleach time. See text for explanations and fitted diffusion coefficients.

rapid recovery (Fig. 6 C), indicating that reversible photobleaching was not detected under the conditions of these experiments. Utilizing the mathematical model, D values were (in cm^2/s × 10^{-7}, n = 5–8): 2.2 ± 0.4 (t_b = 1 ms), 2.7 ± 0.5 (0.6 ms) and 2.9 ± 0.3 (0.2 ms). This calculation assumes that the recovery measured at late time (5 s) is due exclusively to BCECF translational diffusion in the evanescent field. If there is an additional component of fluorescence recovery (as estimated from Fig. 6 C), then calculated D would be greater, up to ~4 × 10^{-7} cm^2/s. The diffusion coefficient for fluorescein in water, measured in a parallel

experiment (Fig. 6 D, $t_{1/2}$ ~0.4 ms), was 2.4 × 10^{-6} cm^2/s; it was shown previously that fluorescein and the acid form of BCECF had the same diffusion coefficients in aqueous solutions (Kao et al., 1993). From these results, averaged cytoplasmic viscosity in membrane-adjacent cytoplasm was 6–10-fold greater than water viscosity. A range is reported here to include the maximum uncertainty in the fractional recovery due to diffusion in the evanescent field. Taken together with the spot photobleaching data, these results indicate that BCECF translation diffusion in membrane-adjacent cytoplasm is significantly slowed compared to that in water, and moderately slowed compared to that in bulk cytosol.

It was assumed in the computation of BCECF diffusion coefficient that there was close contact between the fused silica substrate and the cell surface. However, contact is quite variable for some cells, such as fibroblasts (Lanni et al., 1985; Bicknese et al., 1983), yet close in other cells, such as chicken heart embryonic cells (Gingell et al., 1985). Fig. 7 A (*left*) shows a region of poor contact between the substrate and cell surface in which an aqueous layer (n_r 1.33) of thickness h is present between the fused silica and the cell plasma membrane. It was concluded by Gingell et al. (1987) that such a layer would alter the intensity of the evanescent field in the cytoplasm (n_r 1.38) yet not affect the exponential decay or the distance constant (d) within the cell. Fig. 7 A (*right*) shows the BCECF diffusion coefficient computed from the experimental data in Fig. 6 B (curve for t_b = 0.2 ms) in the presence of an (unrecognized) aqueous layer of thickness (h) between 0 and 100 nm. Interestingly, because d is not affected by the aqueous layer, the computed diffusion coefficient was nearly independent of h. The presence of an aqueous layer does affect the intensity of the evanescent field at the cell surface; for h of 0, 20, 50, and 100 nm, relative intensities were (computed from equations 20 and 24 of Gingell et al., 1987) 1, 0.75, 0.49, and 0.25. These results indicate that the solute diffusion coefficient is insensitive to uncertainties in the details of the cell-substrate contact.

TIR fluorescence imaging was carried out to investigate the nature of the substrate-cell contact, comparing Swiss 3T3 fibroblasts (Fig. 7 B–D, *left*) and MDCK epithelial cells (Fig. 7 B–D, *right*). Whereas BCECF-labeled fibroblasts showed variable substrate contact with distinct regions of focal contact (Fig. 7 B, *left*), the contact appeared relatively uniform for the MDCK cells (Fig. 7 B, *right*). Addition of a large fluorescent dextran (FITC-dextran, 150 kDa) to unlabeled cells was excluded from the region beneath both fibroblasts and MDCK cells (Fig. 7 C). However, a smaller dextran (4 kDa, ~4.4-nm diameter) could penetrate the undersurface of fibroblasts (Fig. 7 D, *left*) but not MDCK cells (Fig. 7 D, *right*). Quantitative image analysis comparing images for 150 kDa versus 4 kDa dextrans indicated that the percentage of FITC-dextran penetrating the undersurface was ~85% for fibroblasts and <30% for MDCK cells. The results suggest close contact between the MDCK cell plasma membrane and fused silica substrate in these studies.
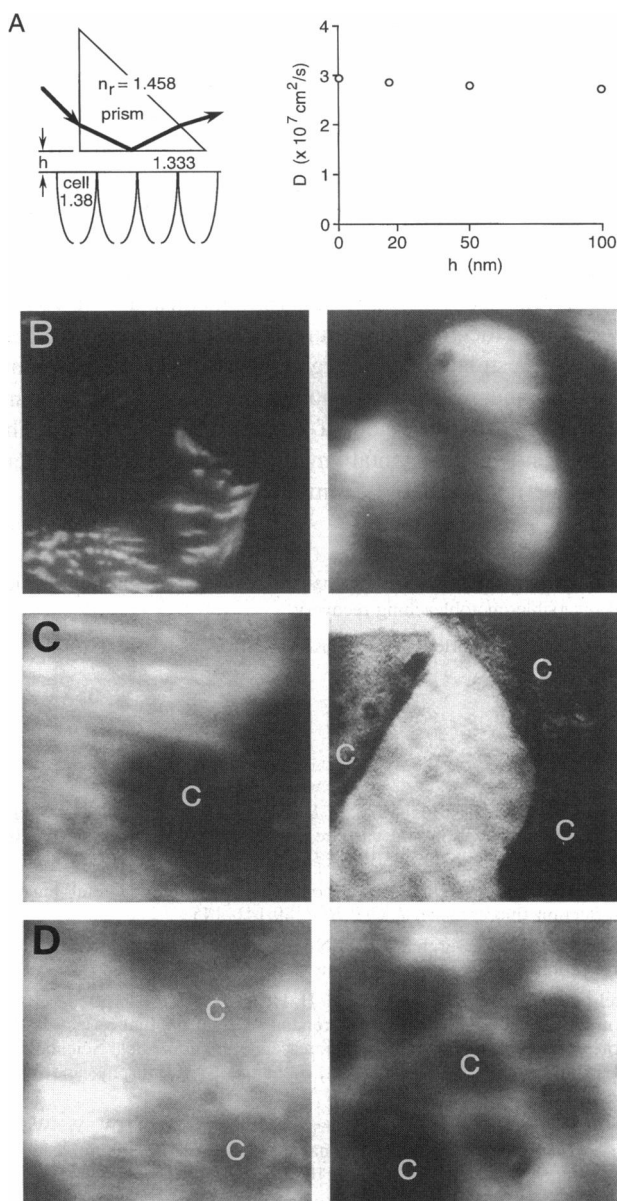
FIGURE 7 Examination of cell-substrate contact. (A) Sensitivity of computed solute diffusion coefficient (D) on the thickness of an aqueous layer (n_r 1.333) between the fused silica coverslip (n_r 1.458) and cell (n_r 1.38). (Left) Schematic of the multilayer geometry. (Right) Diffusion coefficients (computed for parameters t_b = 0.2 ms and d = 112 nm) as a function of the thickness of the aqueous layer (h). The bleach depth varied from 22% (h = 0) to 6% (h = 100 nm) for constant incident intensity. (B) TIR fluorescence image of Swiss 3T3 fibroblasts (left) and MDCK cells (right) labeled with BCECF. Note the focal contacts for fibroblasts and fairly uniform contact for MDCK cells. (C and D) TIR fluorescence images (d = 117 nm) as in B. for unlabeled cells bathed for 15 min in a solution containing FITC-dextran (10 mg/ml; C, 150 kDa; D, 4 kDa). Relatively dark areas where cells are located (some cells labeled c) are observed because of dye exclusion. See text for explanations.

DISCUSSION

TIR-FRAP has been applied previously to measure the on-off kinetics of binding of fluorescent substrates to a glass surface (Axelrod et al., 1986; Hsieh and Thompson, 1994;

Stout and Axelrod, 1994). The small penetration depth of the evanescent field produced by TIR illumination permits relatively selective excitation of substrate-bound fluorophores with little excitation of unbound fluorophores in the bulk aqueous phase (Axelrod, 1981; Gingell et al., 1985). Our study here utilized TIR-FRAP for the first time to measure solute translational diffusion near an interface—the diffusion of BCECF in the cytosol of MDCK cells cultured on quartz coverslips. The biological motivation for this study was to address basic questions about the rheology of membrane-adjacent cytosol as described in the Introduction. The application of TIR-FRAP to measuring solute diffusion was particularly challenging because of the rapid recovery rates, which required very short bleach times and fast data acquisition; the complex time and space dependence of the recovery process, which required the development of a computational model for data analysis; and the presence of a reversible photobleaching process, which required a mechanistic analysis and development of a strategy to eliminate the process.

Several approximations were made in the analysis of TIR-FRAP data. A single-beam incident angle, and thus evanescent field penetration depth, was assumed. The actual beam contained a small spread in incident beam angles because of the objective lens, which was required to increase beam intensity in the sample plane. We believe that the assumption of a single d is justified based on the good agreement between measured and expected diffusion coefficients for fluorophores in aqueous solutions, and the insensitivity of recovery curves to replacement of the 25× objective with 10× and 4× objectives (not shown), in which beam angular spread was reduced, although spot size was increased. A second approximation was the assumption of one-dimensional geometry. For solute diffusion, one-dimensional diffusion was clearly justified because d was much less than the diameter of the laser beam in the sample plane. However, a second-order effect of imperfect x-y uniformity in sample illumination is uncertainty in absolute bleach depth. We believe that the uncertainty in bleach depth had little influence on the quantitative results because of the insensitivity of recovery curve shape to bleach depth (Fig. 4 E), the good agreement between measured and expected diffusion coefficients, and the insensitivity of recovery curve shape to restricting the detection area to the center of the elliptical spot (not shown).

Additional assumptions were required for the analysis of TIR-FRAP data in cells. It was necessary to assume a single effective refractive index for cytosol based on reported measurements (Reichert and Truskey, 1990; Lanni et al., 1985). As discussed previously (Gingell et al., 1987; Bicknese et al., 1993), the assumption of microhomogeneity in the optical properties of cytosol is difficult to evaluate and therefore represents a potential limitation for quantitative analysis of intracellular distances by TIR fluorescence. An additional approximation in cells was the assumption of a single effective evanescent field penetration depth. Whereas cell-substrate contact distance differs considerably across

the undersurface of cultured fibroblasts (Lanni et al., 1985; Bicknese et al., 1983), there was relatively uniform contact for the MDCK epithelial cells grown on a fused silica coverslip (Fig. 7, B–D), similar to findings for chicken embryonic heart cells (Gingell et al., 1985). In addition, because the exponential decay of the evanescent field intensity is not influenced by an aqueous layer between the substrate and plasma membrane (Gingell et al., 1987), the calculated solute diffusion coefficient was insensitive to the details of the cell-substrate contact (Fig. 7 A). Finally, because the decay length of the evanescent field generally used in these studies (~100 nm) was much greater than the membrane thickness (4 nm) and the likely extent of the glycocalyx, the calculated BCECF diffusion coefficient should have been overestimated by no more than 12% (based on calculations utilizing the model). This uncertainty is further reduced by the higher refractive index of the membrane versus the cytosol, so that the actual TIR interface was probably the membrane-cytosol boundary.

An unanticipated problem for the TIR-FRAP measurements in cells was the presence of reversible photobleaching in the time scale of the fluorescence recovery. Reversible photobleaching has been observed previously in photobleaching experiments using various dyes (Velez and Axelrod, 1988; Scalettar et al., 1990; Selvin et al., 1990), including fluorescein (Stout and Axelrod, 1995), and in singlet depletion studies (Johnson and Garland, 1982; Yoshida and Barisas, 1986). Reversible photobleaching has been attributed to the formation and decay of the triplet state based on its oxygen dependence (Johnson and Garland, 1982; Scalettar et al., 1990). Reversible photobleaching was recently identified and characterized in air-saturated viscous solutions; the role of triplet-state relaxation was confirmed by analysis of bleach kinetics and from effects of oxygen and other triplet-state quenchers (Periasamy et al., 1996). The presence of reversible photobleaching in cells is likely due to a combination of reduced oxygen diffusion in the intracellular milieu and BCECF environment effects. Regardless of the exact mechanism, we found that the reversible photobleaching process was effectively eliminated by saturating the bathing solution with 100% oxygen. The observed recovery could then be interpreted in terms of solute translational diffusion.

Notwithstanding these caveats, the results presented here establish the validity of TIR-FRAP for the measurement of solute translational diffusion very near a TIR interface, and provide the first data on solute translational diffusion in membrane-adjacent cytosol. The diffusion of the small polar fluorophore BCECF in membrane-adjacent cytosol was moderately slowed compared to that measured in bulk cytosol by spot photobleaching. We showed previously that fluid-phase viscosity in membrane-adjacent cytosol of MDCK cells was near unity and that most of the BCECF was unbound (Bicknese et al., 1993). From these results and following the theory described in Kao et al. (1993), it is concluded that the slowed BCECF translational diffusion in MDCK cytosol is primarily the consequence of mobile and

immobile "obstacles" in the cytosol (proteins, membranes, etc.). Therefore the density of such nonaqueous obstacles in membrane adjacent cytosol is greater than that in bulk cytosol. Because the data reported here for small fluorophores provide information only on obstacle density without regard to obstacle organization (Furukawa et al., 1991; Kao et al., 1993), further studies of solute diffusion in membrane-adjacent cytosol are needed using larger probe molecules such as FITC-labeled dextrans. Luby-Phelps et al. (1986) reported that large macromolecules are sieved in cytosol by a mechanism presumably involving the cytoskeleton. We postulate that the high density of skeletal elements in membrane-adjacent cytosol should significantly retard the translational diffusion of relatively large solutes. The theory and experimental methodology developed here should permit the direct examination of this hypothesis.

REFERENCES

Ausiello, D. A., J. Hartwig, and D. Brown. 1987. Membrane and microfilament organization and vasopressin action in transporting epithelia. Soc. Gen. Physiol. Ser. 42:259–275.

Axelrod, D. 1981. Cell-substrate contacts illuminated by total internal reflection fluorescence. J. Cell Biol. 89:141–145.

Axelrod, D., T. P. Burghardt, and N. L. Thompson. 1984. Total internal reflection fluorescence. Annu. Rev. Biophys. Bioeng. 13:247–268.

Axelrod, D., R. M. Fulbright, and E. H. Hellen. 1986. Adsorption kinetics on biological membranes: measurement by total internal reflection fluorescence. In Applications of Fluorescence in Biomedical Sciences. D. Lansing Taylor, A. S. Waggoner, F. Lanni, R. F. Murphy, and R. R. Birge, editors. Alan R. Liss, New York. 461–476.

Axelrod, D., D. E. Koppel, J. Schlessinger, E. Elson, and W. W. Webb. 1976. Mobility measurement by analysis of fluorescence photobleaching recovery kinetics. Biophys. J. 16:1055–1069.

Bertch, M. A., and D. E. Koppel. 1988. Fluorescence redistribution after photobleaching—the effect of diffusion during the bleach. Biophys. J. 53:512a. (Abstr.)

Bicknese, S., N. Periasamy, S. B. Shohet, and A. S. Verkman. 1993. Cytoplasmic viscosity near the cell plasma membrane: measurement by evanescent field frequency-domain microfluorimetry. Biophys. J. 65: 1272–1282.

Born, M., and E. Wolf. 1970. Principles of Optics. Pergamon Press, New York. 561–564.

Chandrasekhar, S. 1943. Stochastic problems in physics and astronomy. Rev. Mod. Phys. 15:1–87.

Clegg, J. S. 1984. Properties and metabolism of the aqueous cytoplasm and its boundaries. Am. J. Physiol. 246:R133–R151.

Corbett, J. D., M. R. Cho, and D. E. Golan. 1994. Deoxygenation affects fluorescence photobleaching recovery measurements of red cell membrane protein lateral mobility. Biophys. J. 66:25–30.

Dix, J. A., and A. S. Verkman. 1990. Mapping of fluorescence anisotropy in single cells by ratio imaging: application to cytoplasmic viscosity. Biophys. J. 57:231–240.

Feldberg, S. W. 1969. Digital simulation. A general method for solving electrochemical diffusion-kinetic problems. In Electroanalytical Chemistry, Vol. 3. A. J. Band, editor. Marcell Dekker, New York. 199–296.

Fulton, A. B. 1982. How crowded is the cytoplasm? Cell. 30:345–347.

Furakawa, R., J. L. Arauz-Lara, and B. R. Ware. 1991. Self-diffusion and probe diffusion in dilute and semidilute aqueous solutions of dextran. *Macromolecules.* 24:599–605.

Fushimi, K., J. A. Dix, and A. S. Verkman. 1990. Cell membrane fluidity in the intact kidney proximal tubule measured by orientation independent fluorescence anisotropy imaging. *Biophys. J.* 57:241–254.

Fushimi, K., and A. S. Verkman. 1991. Low viscosity in the aqueous domain of cytoplasm measured by picosecond polarization microscopy. *J. Cell Biol.* 112:719–725.

Gingell, D., O. S. Heavens, and J. S. Mellor. 1987. General electromagnetic theory of total internal reflection fluorescence: the quantitative basis for mapping cell-substratum topography. *J. Cell Sci.* 87:677–693.

Gingell, D., I. Todd, and J. Bailey. 1985. Topography of cell-glass apposition revealed by total internal reflection fluorescence of volume markers. *J. Cell Biol.* 100:1334–1338.

Hecht, E. 1987. Optics. Addison-Wesley Publishing Company, Menlo Park, CA.

Hou, L., F. Lanni, and K. Luby-Phelps. 1990. Tracer diffusion of F-actin and ficoll mixtures—toward a model for cytoplasm. *Biophys. J.* 58: 31–43.

Hsieh, H. V., and N. L. Thompson. 1994. Theory for measuring bivalent surface binding kintics using total internal reflection with fluorescence photobleaching recovery. *Biophys. J.* 66:898–911.

Hsieh, H. V., and N. L. Thompson. 1995. Dissociation kineics between a mouse Fc receptor and IgG—measurement by total internal reflection with fluorescence photobleaching recovery. *Biochemistry.* 34: 12481–12488.

Johnson, P., and P. B. Garland. 1982. Fluorescent triplet probes for measuring the rotational diffusion of membrane proteins. *Biochem. J.* 203:313–321.

Kao, H. P., J. R. Abney, and A. S. Verkman. 1993. Determinants of the translational diffusion of a small solute in cytoplasm. *J. Cell Biol.* 120:175–184.

Kao, H. P., and A. S. Verkman. 1996. Construction and performance of a FRAP instrument with microsecond time resolution. *Biophys. Chem.* 59:203–210.

Lanni, F., A. S. Waggoner, and D. L. Taylor. 1985. Structural organization of interphase 3T3 fibroblasts studied by total internal reflection fluorescence microscopy. *J. Cell Biol.* 100:1091–1102.

Lepock, J. R., K. H. Cheng, S. D. Campbell, and J. Kruuv. 1983. Rotational diffusion of tempone in the cytoplasm of Chinese hamster lung cells. *Biophys. J.* 44:405–412.

Lopez, A., L. Dupou, A. Altibelli, J. Trotard, and J. F. Tocanne. 1988. Fluorescence recovery after photobleaching (FRAP) experiments under conditions of uniform disk illumination. *Biophys. J.* 53:963–970.

Luby-Phelps, K. 1994. Physical properties of cytoplasm. *Curr. Opin. Cell Biol.* 6:3–9.

Luby-Phelps, K., S. Mujundar, R. Mujundar, L. Ernst, W. Galbraith, and A. Waggoner. 1993. A novel fluorescence ratiometric method confirms the low solvent viscosity of the cytoplasm. *Biophys. J.* 65:236–242.

Luby-Phelps, K., D. L. Taylor, and F. Lanni. 1986. Probing the structure of cytoplasm. *J. Cell Biol.* 102:2015–2022.

Mastro, A. M., and A. D. Keith. 1984. Diffusion in the aqueous compartment. *J. Cell Biol.* 99:180s–187s.

Parsegian, V. A., and D. C. Rau. 1984. Water near intracellular surfaces. *J. Cell Biol.* 99:196s–200s.

Periasamy, N., S. Bicknese, and A. S. Verkman. 1996. Reversible photobleaching of fluorescein conjugates in air-saturated viscous solutions: molecular tryptophan as a triplet state quencher. *Photochem. Photobiol.* 63:265–271.

Periasamy, N., H. P. Kao, and A. S. Verkman. 1992. Organic osmolytes increase cytoplasmic microviscosity in kidney cells. *Am. J. Physiol.* 263:C901–C907.

Porter, K. R. 1984. The cytomatrix: a short history of its study. *J. Cell Biol.* 99:3s–12s.

Reichert, W. M., and G. A. Truskey. 1990. Total internal reflection fluorescence (TIRF) microscopy. I. Modelling cell contact region fluorescence. *J. Cell Sci.* 96:219–230.

Scalettar, B. A., P. R. Selvin, D. Axelrod, M. P. Klein, and J. E. Hearst. 1990. A polarized photobleaching study of DNA reorientation in agarose gels. *Biochemistry.* 29:4790–4798.

Selvin, P. R., B. A. Scalettar, J. P. Langmore, D. Axelrod, M. P. Klein, and J. E. Hearst. 1990. A polarized photobleaching study of chromatin reorientation in intact nuclei. *J. Mol. Biol.* 214:911–922.

Song, L., E. J. Hennink, I. T. Young, and H. J. Tanke. 1995. Photobleaching kinetics of fluorescein in quantitative fluorescence microscopy. *Biophys. J.* 68:2588–2600.

Stout, A. L., and D. Axelrod. 1994. Reversible binding kinetics of a cytoskeletal protein at the erythrocyte submembrane. *Biophys. J.* 67: 1324–1334.

Stout, A. L., and D. Axelrod. 1995. Spontaneous recovery of fluorescence by photobleached surface-adsorbed proteins. *Photochem. Photobiol.* 62: 239–244.

Thomas, A. P., D. C. Renard, and T. A. Rooney. 1991. Spatial and temporal organization of calcium signalling in hepatocytes. *Cell Calcium.* 12:111–126.

Thompson, N. L., H. M. McConnell, and T. P. Burghardt. 1984. Order in supported phospholipid monolayers detected by the dichroism of fluorescence excited with polarized evanescent illumination. *Biophys. J.* 46:739–747.

Velez, M., and D. Axelrod. 1988. Polarized fluorescence photobleaching recovery for measuring rotational diffusion in solutions and membranes. *Biophys. J.* 53:575–591.

Verkman, A. S. 1991. New microfluorimetry approaches to examine cell dynamics. *Comments Mol. Cell. Biophys.* 7:173–187.

Verkman, A. S., M. Armijo, and K. Fushimi. 1991. Construction and evaluation of a frequency-domain epifluorescence microscope for lifetime and anisotropy decay measurements in subcellular domains. *Biophys. Chem.* 40:117–125.

Yoshida, T. M., and B. G. Barisas. 1986. Protein rotational motion in solution measured by polarized fluorescence depletion. *Biophys. J.* 50: 41–53.

Zen, K., J. Biwersi, N. Periasamy, and A. S. Verkman. 1992. Second messengers regulate endosomal acidification in Swiss 3T3 fibroblasts. *J. Cell Biol.* 119:99–110.